Carbohydrate Polymers 156 (2017) 470–480

Contents lists available at ScienceDirect

Carbohydrate Polymers

journal homepage: www.elsevier.com/locate/carbpol

Structural features of heparanase-inhibiting non-anticoagulant heparin derivative Roneparstat

Anna Alekseeva[a,*], Giulia Mazzini[b], Giuseppe Giannini[c], Annamaria Naggi[a,b]

[a] Centro Alta Tecnologia Istituto di Ricerche Chimiche e Biochimiche G. Ronzoni, srl, via G. Colombo, 81, 20133 Milan, Italy
[b] Istituto di Ricerche Chimiche e Biochimiche G.Ronzoni, via G. Colombo, 81, 20133 Milan, Italy
[c] Sigma-Tau Industrie Farmaceutiche Riunite S.p.A, Via Pontina, Km. 30,400, 00040 Pomezia, Italy

ARTICLE INFO

Article history:
Received 2 June 2016
Received in revised form 5 September 2016
Accepted 12 September 2016
Available online 13 September 2016

Keywords:
Glycol-split
Heparin
Anti-cancer
Non-anticoagulant
Heparanase

ABSTRACT

Owing to their anti-tumor and anti-inflammatory properties, non-anticoagulant glycol-split (gs) heparins, obtained by periodate oxidation/borohydride reduction, are of growing interest. The present study was focused on the structural characterization of N-acetylated gs-heparin Roneparstat, a promising anti-cancer heparanase-inhibiting drug currently being investigated in clinical trials. The major and minor structural features of structurally complex Roneparstat have been characterized for the first time using conductimetric titration, size-exclusion chromatography with triple detector array, NMR and LC/MS. It has been shown that gs-uronic acids are mainly interspersed by unmodified disaccharide building blocks, but can also be present within sequences with consequent gs-residues. Peculiar gs-sequences, such as those derived from antithrombin binding regions and those containing I_{2S}-A_{NS3S6S}, as well as a variety of unnatural terminal groups, markers of preparation processes, have also been identified in Roneparstat. Structural features of Roneparstat that may play an important role in interactions with proteins have been summarized.

1. Introduction

Heparanase, an endoglycosidase confined inside specific cells under normal conditions, is overexpressed in most human oncological diseases, promoting tumor metastasis and angiogenesis (Pisano, Vlodavsky, Ilan, & Zunino, 2014; Vlodavsky & Friedman, 2001). The mechanism of its action under pathological conditions is believed to be associated with the release of physiologically and pathologically important molecules (growth factors, cytokines, chemokines and other proteins). Their release is facilitated in tumors by heparanase, degrading heparan sulfate (HS) chains of HS proteoglycans on cell surfaces and within the extracellular matrix (ECM) (Vlodavsky & Friedman, 2001). HS/heparanase interactions have generated interest as target for anti-cancer therapy. The crystal structure of heparanase, recently published, is expected to further stimulate interest in the investigation and design of its inhibitors (Wu, Viola, Brzozowski, & Davies, 2015). Among current approaches used for heparanase inhibition (Ferro et al., 2007; Ferro et al., 2012), development of heparin derivatives, e.g.glycol-split (gs) heparins (Mousa, Linhardt, Francis, & Amirkhosravi, 2006; Ritchie et al., 2011) as HS mimics, is of considerable interest.

Heparin is a polydisperse, linear, highly sulfated glucosaminoglycan (GAG), consisting of *uronic acid – glucosamine* repeating disaccharide building blocks with different sulfation and acetylation degrees, which vary in heparins of different origin. In spite of these variations, some structural features are considered common to heparins from all sources (Casu & Lindahl, 2001; Fu et al., 2013; Yates et al., 1996; Zhang et al., 2011). The trisulfated disaccharide A_{NS6S} – I_{2S} (N-sulfated D-glucosamine-6-*O*-sulfate – 2-O-sulfated L-iduronic acid) is the prevalent building block present within highly sulfated regions (Casu, 2005), while the disaccharide A_{NAc} – G (N-acetyl-D-glucosamine – D-glucuronic acid) is the main constituent of the undersulfated sequences of heparin (Yamada, Yamane, Tsuda, Yoshida, & Sugahara, 1998). D-Glucuronic acid followed by a trisulfated glucosamine A_{NS3S6S} (N-sulfated D-glucosamine-3,6-*O*-disulfate), formed at the last biosynthesis step

Abbreviations: gs, glycol-split; LMWH, low-molecular weight heparin; U, uronic acid; I, L-iduronic acid; G, D-glucuronic acid; I_{2S}, L-iduronic acid 2-O-sulfate; A_{NS6S}, D-glucosamine-N,6-O-disulfate; A_{NAc}, N-acetylated D-glucosamine; A_{NS3S6S}, D-glucosamine N,3-O,6-O-trisulfate; ΔU_{2S}, 4,5-unsaturated uronic acid 2-O-sulfate; R, remnant of the gs-uronic acid; Gal, D-galactose; Xyl, D-xylose; Ser, L-serine; ATBR, antithrombin-binding region; RE, reducing end; NRE, non-reducing end; LR, linkage region.

* Corresponding author.
E-mail addresses: anna.v.alekseeva@gmail.com (A. Alekseeva), giulia.mazzini@gmail.com (G. Mazzini), Giuseppe.Giannini@sigma-tau.it (G. Giannini).

http://dx.doi.org/10.1016/j.carbpol.2016.09.032
0144-8617/

within some heparin chains, is the marker of the pentasaccharide sequence A_{NAc6S}-**G-A**$_{NS3S6S}$-I_{2S}-A_{NS6S} and its variants (Loganathan, Wang, Mallis, & Linhardt, 1990; Naggi et al., 2016). These sequences, interacting with antithrombin, largely determine the anticoagulant activity of heparin. A linkage region (LR) G-$(Gal)_2$-Xyl-Ser tetrasaccharide can be also present at the reducing end (RE) of some heparin chains (Iacomini et al., 1999). This particular sequence, susceptible to treatments used during industrial heparin API preparation, usually varies within the range 1.0–1.3% (Zhang et al., 2011).

These and other minor constituents give rise to the structural microheterogeneity of heparin and may contribute to the wide variety of interactions with different biomolecules (Shriver, Capila, Venkataraman, & Sasisekharan, 2012). At the same time, such variety significantly complicates structural characterization of heparin-related compounds.

Heparin represents a good candidate for developing anti-cancer products, including heparanase inhibitors, due to its commercial availability and structural similarity with HS, the natural substrate for heparanase. In fact, several new therapeutic uses of heparins and low molecular weight heparins (LMWHs) have been envisaged in various fields, including inflammation and cancer (Lever & Page, 2002; Mousa & Petersen, 2009). To reduce the risks of bleeding that limit the anti-cancer and anti-inflammatory uses of heparins, inactivation of their antithrombin binding region (ATBR) is required. Even though they are efficient and selective, enzymatic digestion (Xiao et al., 2011) or affinity chromatography (Höök, Björk, Hopwood, & Lindahl, 1976) are time consuming and expensive methods for the inactivation or removal of the ATBR-containing chains. Glycol-splitting of uronic acid residues, including the essential glucuronic acid of the pentasaccharide A_{NAc6S}-G-A_{NS3S6S}-I_{2S}-A_{NS6S} (Fig. 1), by periodate oxidation represents an alternative way of reducing anticoagulant properties, without impairing other biological activities (Mousa et al., 2006; Naggi et al., 2005; Ritchie et al., 2011; Zhou et al., 2011).

It has been shown that heparanase-inhibitory activity of gs-heparins is strictly related to the content of gs-uronic acid residues as well as to the degree N-sulfation and N-acetylation (Naggi et al., 2005). Glycol-splitting of unfractionated heparin increases heparanase inhibition due to additional conformational flexibility introduced by more freely rotating gs-residues (Casu & Naggi, 2003). N-desulfated N-acetylated gs-heparins were shown to possess heparanase-inhibitory activity similar to that of N-sulfated gs-heparins. However, N-acetylated derivatives induced lower release of FGF-2 growth factor, possessing mitogenic activity, from ECM (Naggi et al., 2005). These properties, together with the lack of anticoagulant activity, made such compounds attractive for targeting heparanase in cancer treatments. In fact, N-desulfated and N-acetylated gs-heparins emerged as highly effective and specific inhibitors of heparanase, tumor growth and metastasis *in vitro* (Achour et al., 2016; Naggi et al., 2005) and *in vivo* (Casu, Vlodavsky, & Sanderson, 2007; Ritchie et al., 2011). Among those, ***SST0001*** (Roneparstat; Sigma-Tau Research, Switzerland) is a gs-heparin, obtained by periodate oxidation/borohydride reduction of totally N-desulfated and N-acetylated heparin, possessing anti-tumor activity arising from its high heparanase-inhibiting activity (Ritchie et al., 2011). Roneparstat is being currently tested in Phase I clinical trials for the treatment of multiple myeloma.

Despite the fact that the anti-cancer activity of SST0001 has been proven, structural features of this heparin derivative, including properties potentially relevant for its activity, have not been studied in detail. Based, on the data obtained for N-sulfated gs-heparins/gs-LMWHs (Alekseeva, Casu, Torri, Pierro, & Naggi, 2013; Alekseeva et al., 2014a) its structure is shown schematically in Fig. 1. The challenges in structural characterization, and especially in elucidation of particular sequences important for Roneparstat binding with proteins, are related to the above mentioned heparin microheterogeneity, as well as high molecular weight and polydispersity (Shriver et al., 2012). Side reactions, such as hydrolysis (Conrad & Guo, 1992) can additionally increase the structural complexity of gs-heparins.

In the present study, we for the first time report structural features of SST0001 determined using various analytical methods: conductimetric titration (Casu & Gennaro, 1975); size exclusion chromatography with triple detector array (Bertini, Bisio, Torri, Bensi, & Terbojevich, 2005); high resolution techniques, widely used for heparin characterization, such as mono- and bidimensional NMR (Fu et al., 2013; Guerrini, Naggi, Guglieri, Santarsiero, & Torri, 2005) and LC/MS analysis (Langeslay et al., 2013; Naimy, Leumarie, Bowman, Costello, & Zaia, 2008; Thanawiroon, Rice, Toida, & Linhardt, 2004). For the latter, the ion pair reversed phase chromatography (IP-RP-HPLC) with electrospray ionization mass spectrometry (ESI–MS), developed in our previous studies for gs-heparins (Alekseeva et al., 2013), was adapted for the characterization of the heparinase-generated oligosaccharides of Roneparstat.

2. Experimental

2.1. Materials and reagents

The starting porcine mucosal heparin sodium salt was from Opocrin, Heparin lyases I (EC4.2.2.7), II, III (EC4.2.2.8) were from Grampian Enzymes, and disaccharide standards were from Iduron. Sodium chloride (>99.5%), sodium periodate (>99%), dibutylamine (DBA, >99.5%), methanol (LC–MS grade), acetic acid (glacial, 99.9%), formic acid (98–100%) were purchased from Sigma-Aldrich. Volumetric solutions of sodium hydroxide 0.1 N and sodium borohydride (95%) were from Riedel-de Haën. Solid sodium hydroxide (>99%) and sodium acetate were from Merck, calcium acetate (>97%), from BDH. Deionized water was prepared with an osmosis inverse system (conductivity less than 0.06 μS), filtered (Millipore filter 0.22 μm) and used for sample dilution and mobile phases.

2.2. Preparation of SST0001

Glycol-split derivative of N-acetylated porcine mucosal heparin (SST0001, Roneparstat) was prepared by consecutive N-desulfation, N-acetylation and further periodate oxidation/borohydride reduction, as previously reported (Naggi et al., 2005).

2.3. Conductimetric titration

Sulfation degree, expressed as the *sulfate-to-carboxylate* molar ratio, was determined by conductimetric titration (Casu & Gennaro, 1975). The analyses were performed on an automatic titrator "Titrando" 888 ("Metrohn") coupled with a Metrohm Conductimeter 712 with a conductivity cell characterized by a constant 0,76 cm^{-1}. An aqueous solution (55–60 ml) of each sample (~40 mg), previously exchanged on an activated Amberlite IR-120(H+) column (12 ml), was titrated by adding point by point 75 μl of 0.1 M NaOH solution, and the conductivity value was recorded after 160–200 s of every aliquot addition to reach the solution equilibrium.

2.4. SEC-TDA analysis

Determination of the molecular weight distribution and Mark-Houwink parameters was performed by HP-SEC-TDA on a Viscotek (Houston, Texas) instrument equipped with a triple detector array 302 with refraction index (RI) detector, viscometer, and light-scattering (90° and 7°) detector. SEC separation was performed on

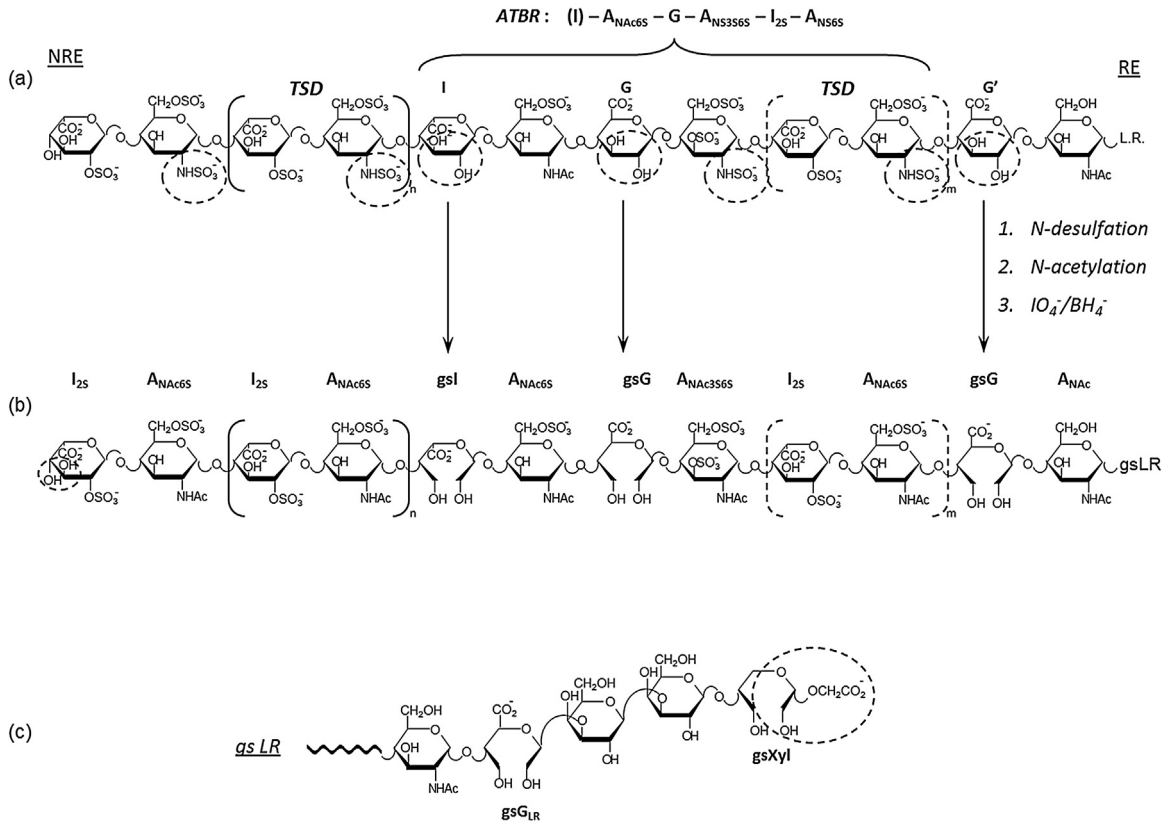

Fig. 1. Structure of heparin and Roneparstat (SST0001) obtained by N-desulfation, N-acetylation and subsequent periodate/borohydride treatment (adapted from (Alekseeva et al., 2014a)).
(a) – heparin chains, (b) – SST0001 chains, (c) – glycol-split linkage region that may be present at the RE of some chains.
Circled residues are those susceptible to N-desulfation, N-acetylation, periodate oxidation/borohydride reduction or hydrolytic side reactions.

G2500 and G3000 (7.8 mm x 30 cm TSK GMPWxl) Tosoh columns with 0.1 M $NaNO_3$ as eluent at a flow-rate 0.6 ml/min, by injecting 100 μl of 5 mg/ml solution of each samples. Peak integration and data processing were performed using OMNISEC 4.1 software. The Mark-Houwink parameters *a* and *logK*, as well as hydrodynamic radius (Rh), were calculated from the whole Mw range using OMNISEC 4.1.

2.5. ^{13}C NMR and HSQC NMR

^{13}C NMR spectra were recorded on a Bruker Avance 500 MHz (125 MHz for ^{13}C) spectrometer (Karlsruhe, Germany), equipped with a 10-mm BBO multi-nuclear probe, using a Bruker pulse program zgig. The spectra were acquired with relaxation delay 1 s, acquisition time 0.327 s, spectral width 299 ppm. The temperature was 313 K and the applied transient number was 20400. The transmitter frequency off-set was 90 ppm. The spectrum size used was 128k with zero filling. Before Fourier transformation line broadening of 4 Hz was applied to decrease noise.

HSQC NMR spectra were recorded on a Bruker Avance 500 MHz spectrometer (Karlsruhe, Germany), equipped with a 5-mm TCI cryoprobe, in phase-sensitive, sensitivity pure-absorption mode with decoupling in the acquisition period (Bruker pulse program hsqcetgpsisp.2). The J_{C-H} coupling constant was set to 150 Hz. Spectra were recorded using a spectral width of 8 ppm and 80 ppm in the proton and carbon dimensions, respectively. The carrier frequencies for proton and carbon were 4.7 ppm and 80 ppm. Spectra were acquired into a time domain of 1024 complex points, using from 16 to 32 scans for each of 320 increments. The relaxation delay and the acquisition time were set at 2 s and 0.178 s, respectively. The matrix size of 1024 × 320 data points was zero filled to 4096 × 2048 and a squared cosine function was applied prior to Fourier transformation.

Integration of peak volumes in the HSQC spectra was made using standard Bruker TOPSPIN 3.0 software. Sample solutions of 250 mg/ml and 5–10 mg/ml in D_2O were used for the ^{13}C NMR and HSQC NMR, respectively.

2.6. IPRP-HPLC/ESI-TOF-MS analysis of the enzymatically depolymerized samples

The samples (100 μg each) of the starting heparin and SST0001 were enzymatically depolymerized by heparinases I, II and III, as well as heparinase II along, as described in (Alekseeva et al., 2014a).

LC–MS analyses were carried out on a HPLC system (Ultimate 3000, Dionex) coupled with an ESI-Q-TOF mass-spectrometer (microqTOF, Bruker Daltonics). The chromatographic separation was performed using a Kinetex C18 analytical column (100 × 2.1 mm I.D., 2.6 μm particle size, Phenomenex). Eluent A (10 mM DBA, 10 mM CH_3COOH in water) and eluent B (10 mM DBA and 10 mM CH_3COOH in methanol) were delivered at 0.1 ml/min. The separation gradient was optimized for the separation of N-acetylated oligosaccharides: the solvent composition was held at 10% B for the first 5 min, then increased to 35% B over 30 min, and to 60% B over further 50 min; afterwards, the content of eluent B was increased to 90% in 3 min, and held for 5 min. Finally, it was returned to 10% B over 2 min, and held for the last 20 min for equilibrating the chromatographic column before the injection of the next sample. The injection volume was 5 μl.

MS detection was performed using the following parameters: ESI in negative ionization mode, drying gas temperature +180 °C and flow-rate 7.0 l/min, nebulizer pressure 0.9 bar; and capillary

voltage +3.2 kV. The mass spectra of the oligosaccharides were acquired in a full scan mode (m/z scan range 200–2000). An external calibration method using sodium formate clusters as calibrants was used to achieve a good accuracy: the major species were detected with the accuracy < 5 ppm.

2.7. Multi-step isolation of pentasulfated mono-glycol-split-tetrasaccharide

The first-step fractionation of a gs-heparin digested with heparinases was performed using size exclusion chromatography as previously described (Alekseeva et al., 2014a) for the gs-oligomers generated from gs-enoxaparin. The collected tetrasaccharide fraction was then sub-fractionated by IPRP-HPLC in order to isolate the major tetrasaccharide ΔU_{2S}-A_{NS6S}-gsG-A_{NS6S}. The separation was carried out on a preparative HPLC/UV system "Knauer Smartline 1000" using a C18 Knauer column (250 × 8 mm, 5 μm), isocratic elution (10 mM DBA, 10 mM CH_3COOH in H_2O—CH_3OH = 43:57 (v/v)) at a flow-rate 2.5 ml/min, and UV monitoring at 232 nm. A fraction eluted within the range of RT 49–52 min was collected and dialyzed using a 100–500 Da cut-off membrane in order to eliminate the excess of DBA acetate. Following desalting, the samples were freeze-dried and characterized by NMR and LC–MS. NMR was performed as described above, while LC/MS analysis was carried out using the previously published method (Alekseeva et al., 2013).

3. Results

3.1. Coductimetric titration

The conductimetric titration method, introduced in 1975 for heparin samples (Casu & Gennaro, 1975), was applied for monitoring the **sulfation degree**. The calculated molar *sulfate-to-carboxylate* (SO_3^-/COO^-) ratios are reported in Table 1 for both the starting heparin and SST0001. As expected, *N*-acetylated gs-heparin (SST0001) is characterized bya *sulfate-to-carboxylate* ratio (1.3, Table 1) that is 30% lower than for the starting heparin (1.9, Table 1). Considering that heparin chains comprise mainly trisulfated disaccharide, conductimetric results confirm that the starting heparin was almost completely N-desulfated More accurate measurement of the residual N-sulfation was conducted using NMR (see 3.3).

3.2. SEC-TDA analysis

Since chemical treatments used for the preparation of SST0001 can cause side reactions, such as hydrolysis of gs-residues or even glycosidic bonds, monitoring the **molecular weight** and **polydispersity** was considered one of the key steps in the characterization of SST0001. Table 1 reports the peak molecular weight (Mp), weight average molecular weight (Mw) and polydispersity index (D = Mw/Mn, where Mn is number average molecular weight) values (Bertini et al., 2005) describing the entire molecular weight distribution of both heparin and SST0001. Both samples show a single symmetric peak in the refractor index chromatographic profile at retention time of about 12 min (Fig. S1) indicating that the reactions did not significantly affect polydispersity (1.4 for both samples,Table 1). Notably, each molecular weight parameter (Mp, Mw and Mn) decreased for 14–15% (Table 1) in agreement with the loss of one sulfate group (in its sodium salt form) per disaccharide unit. These data suggest that no significant hydrolysis at the level of gs-residues occurred (Alekseeva et al., 2013; Conrad & Guo, 1993).

SEC coupled with a TDA system allowed not only the molecular weight distribution but also **hydrodynamic properties** of the analyzed samples to be monitored through Rh and the Mark-Houwink parameters *a* and *logK* (Table 1). These latter, easily evaluated from the data concerning intrinsic viscosity as a function of molecular weight ($log[\eta] = logK + a \cdot logM$), describe conformational changes in polymers (Wagner, 1985), e.g. more rigid polymers are characterized by higher absolute values of *a* and *logK*. Table 1 shows that, together with the decrease of Rh (from 3.9 to 3.4 nm), absolute values of Mark-Houwink parameters also decreased for SST0001 with respect to the starting heparin. Given the absence of any hydrolytic processes, lower Rh could be explained by a more compact structure of SST0001 with respect to the starting heparin. The higher conformational flexibility is likely to be caused by two factors, lower sulfation degree (as shown by conductimetry) and the presence of gs-residues. For the N-acetylated heparin derivative both *a* and *logK* values (0.90 and 4.50, respectively, *not shown in* Table 1) were found between those of the starting heparin (0.92 and 4.60, Table 1) and SST0001 (0.87 and 4.42, Table 1). These values indicate that N-desulfation followed by N-acetylation facilitate the formation of more compact random coil of polysaccharide chains as the result of lower negative charge. Further size decreases of polysaccharide chains following glycol-splitting is likely to be caused by the increased local mobility of gs-residues, acting as flexible joints along the SST0001 chains.

3.3. Mono- (^{13}C) and bidimensional (HSQC) NMR

Mono- and bidimensional NMR, the most commonly used techniques for GAGs characterization and differentiation (Fu et al., 2013; Guerrini et al., 2005), have been applied for qualitative evaluation of the spectra as well as for the quantitative analysis of **monosaccharide composition** of both the starting heparin and SST0001.

As shown in Fig. 2, the majority of the signals in the ^{13}C NMR spectra are well-separated and reflect the major chemical modifications introduced into heparin chains during SST0001 preparation. Almost all of the signals associated with the heparin A_{NS} residue (A_{NS}-(I_{2S}) C1 at 99.6 ppm, I_{2S}-(A_{NS}) C1 at 102.2 ppm, A_{NS} C2 at 60.8 ppm, A_{NS3S} C2 at 59.5 ppm, Fig. 2a) disappeared from the ^{13}C NMR spectrum of SST0001 because of N-desulfation (Fig. 2b).

The peak at 65.4 ppm, associated with C3 signal of I_{2S} followed by A_{NH2} (Yates et al., 1996), and the C2 signal of A_{NH2} (57.1 ppm), characteristic for *N*-desulfated heparin derivative, are absent in the SST0001 spectrum (Fig. 2b). The absence of A_{NH2} signals, together with the appearance of a strong A_{NAc} C2 signal (56.2 ppm, Fig. 2b) indicates the complete *N*-acetylation. A_{NAc} followed by G (99.8 ppm, Guerrini et al., 2005) is absent in the SST0001 spectrum because of the oxidation of glucuronic acid. Accordingly, new signals at 98.0 and 99.0 ppm, corresponding to the A_{NAc} followed by gsI and gsG respectively (Alekseeva et al., 2014a), appeared in its spectrum. The periodate/borohydride treatment, in fact, leads to the complete splitting of non-sulfated glucuronic and iduronic acids: the signals of I and G (103.5-105.5 ppm, Guerrini et al., 2005) disappeared, and the signals corresponding to the gsresidues gsG and gsI (106–107 ppm, (Alekseeva et al., 2014a)) appeared in the spectrum of SST0001 (Fig. 2).

Relative signal areas are proportional to the molar ratios of the corresponding units (Desai & Linhardt, 1995; Guerrini, Bisio & Torri, 2001). However, several signals in monodimensional ^{13}C NMR spectra of heparin and SST0001 overlapped, so that this method could not be used for quantitative analysis. To obtain more informative and resolved spectra 2D HSQC NMR was applied (Figs. 3 and S2, Table 2). This method was previously optimized for the quantitative analysis of heparins (Guerrini et al., 2005) and LMWHs (Guerrini, Guglieri, Naggi, Sasisekharan, & Torri, 2007) and also applied for gs-heparins and gs-LMWHs (Alekseeva et al., 2013; Alekseeva et al., 2014a).

The assignment of the cross-peaks observed in the 2D HSQC NMR spectra (Figs. 3 and S2) relied on published data (Guerrini

Table 1
Sulfate-to-carboxylate ratios, obtained by conductimetry, and SEC-TDA data for the starting heparin and Roneparstat (SST0001) samples.

Sample	Conductimetric titration	SEC-TDA					
	SO_3^-/COO^- ratio	Molecular weight distribution			Mark-Houwink parameters		Rh, nm
		Mp, kDa	Mw, kDa	D (Mw/Mn)	a	logK	
Heparin	1.9	17.2	19.5	1.4	0.92	−4.60	3.9
SST0001	1.3	14.8	16.6	1.4	0.87	−4.42	3.4

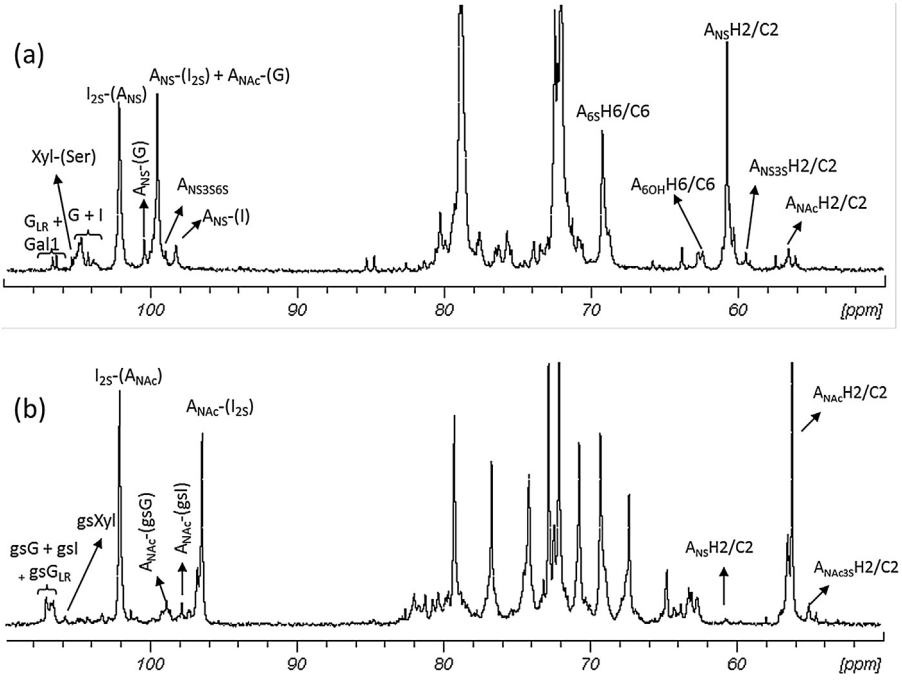

Fig. 2. ^{13}C NMR spectra of the starting porcine mucosal heparin (a) and SST0001 (b).
I_{2S} – 2-O-sulfated iduronic acid, I/G – non-sulfated iduronic/glucuronic acid, gsI/gsG/gsXyl – glycol-split iduronic/glucuronic acid/xylose, A_{NS}/A_{NAc} – N-sulfated/N-acetylated glucosamine, A_{6S} – 6-O-sulfated glucosamine, G_{LR} – glucuronic acid within linkage region (LR), Xyl – xylose, Gal – galactose, Ser – serine.

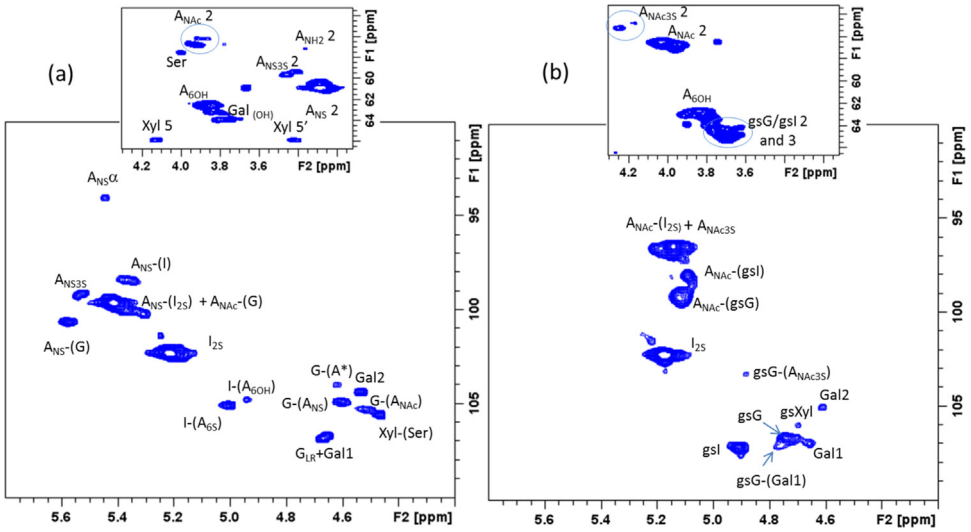

Fig. 3. Characteristic anomeric region, as well as H2/C2 ring region, of the 2D HSQC NMR spectra of the starting porcine mucosal heparin (a) and SST0001 (b).
I_{2S} – 2-O-sulfated iduronic acid, I/G – non-sulfated iduronic/glucuronic acid, gsI/gsG/gsXyl – glycol-split iduronic/glucuronic acid/xylose, A_{NS}/A_{NAc} – N-sulfated/N-acetylated glucosamine, A_{6S} – 6-O-sulfated glucosamine, G_{LR} – glucuronic acid within linkage region (LR), Xyl – xylose, Gal – galactose, Ser – serine.

et al., 2005; Yates et al., 1996) for heparins and our recent reports for gs-heparins (Alekseeva et al., 2013, 2014a). As in the case of monodimensional ^{13}C NMR, the 2D spectra are characteristic for each analyzed sample and reflect the major chemical modifications introduced at each preparation step. Notably, several signals that overlapped in the ^{13}C NMR spectra are well-separated in the 2D HSQC NMR spectra (Fig. 3), e.g. gsI (4.94/106.9 ppm) and gsG (4.71/106.7 ppm). Additionally, minor signals of gsLR

Table 2
Molar monosaccharide composition of heparin and SST0001 determined by 2D HSQC NMR.

Heparin	A_{NS}	A*	A_{NAc}	A_{NH2}	I_{2S}	I-A_{6S}	I-A_{6OH}	G-A*	G-A_{NS}	G-A_{NAc}	Gal1+G	Gal2	Xyl-Ser
	81.1	6.4	11.4	1.1 (<LOQ)	76.6	6.2	2.1	2.4	6.7	6	7.8	4.4	5.3
SST0001	A_{NS}	A*	A_{NAc}	A_{NH2}	I_{2S}	gsI	gsG-A*	gsG	G/I	gsG-Gal	Gal1	Gal2	gsXyl-Serox
	1.6 (<LOQ)	5	91.3	<LOD	74.7	8.6	2.1	11.1	<LOD	3.5	4	2.5	1.9

A* – trisulfated glucosamine residue (A_{NS3S6S} in heparin; $A_{NAc3S6S}$ in SST0001).
LOD: signal-to-ratio = 3, LOQ: signal-to-ratio = 10.
Glucosamine molar ratio was calculated from the H2/C2 cross-peak, the uronic acids content was determined using their anomeric residues.

residues (gsG_{LR} at 4.92/107.6 ppm, Gal1 at 4.66/106.9 ppm, Gal2 at 4.61/105.0 ppm, gsXyl at 4.75/105.6 ppm) are also observed (Fig. 3b).

The data of monosaccharide compositional analysis are reported in Table 2. The glucosamine content was evaluated using the volumes of H2/C2 cross peaks, while uronic acid quantitative analysis was performed using the better resolved H1/C1 signals (Fig. 3). The method permitted the evaluation of the content of different glucosamine and uronic acid residues, including residual signals of A_{NS} in SST0001 (1.6 molar%), as well as different types of gs-units (gsI, gsG followed by A_{NAc}, gsG followed by 3-O-sulfated A_{NAc}, LR related gsG followed by Gal monosaccharide, gsXyl generated by oxidation of LR xylose). The gsXyl content (1.9 molar%) appears lower than for gsG-(Gal) (3.5 molar%) indicating partial erosion of this terminal gs-fragment from the gsLR sequence. It is also worth noting that the content of Gal2 residue (followed by Xyl in LR) is slightly lower than Gal1. This discrepancy could indicate that hydrolytic side reactions, occurring during SST0001 preparation, could lead to partial erosion not only of gsXyl but also one Gal residue. The corresponding hypothetic structures were not detected by NMR nor by LC/MS analysis, probably because of their very low abundance.

3.4. LC/MS analysis of heparinase-generated oligosaccharides

Oligosaccharides obtained by heparinase cleavage were analyzed by the IPRP-HPLC/ESI-Q-TOF method for the **in-depth study ofchemical modifications** introduced into heparin chains during SST0001 preparation. Owing to their substrate specificity well-studied for heparin/LMWH substrates (Shriver et al., 2000; Wang, Buhse, Al-Hakim, Boyne Ii, & Keire, 2012; Xiao et al., 2011; Yu et al., 2000), heparinases were expected to preferentially cleave glycosidic bonds of unmodified heparin sequences, skipping those containing gs-residues (Alekseeva et al., 2013). This would provide information concerning heparin sequences as well as minor modifications introduced by chemical treatment during preparation of Roneparstat. The specificity of heparinases largely depends on the sulfation/acetylation pattern of the heparin/HS substrate. Heparinase I, specific for highly sulfated regions of heparin/HS at A_{NS}-I_{2S} linkages, as well as heparinase III, acting prevalently at the glycosidic linkages A_{NAc}– U (where U is a non-sulfated uronic acid, I or G), were expected to act only on unmodified heparin, but not on SST0001. Heparinase II, cleaving glycosidic linkages between A_{NS}/A_{NAc} and uronic acid, either I_{2S} or I/G, (Wang et al., 2012) was expected to provide the most complete digestion of both heparin and SST0001. Accordingly, both samples were exhaustively digested in duplicate with only heparinase II and the mixture of heparinases I, II and III. As shown in Fig. S3, the addition of heparinases I and III does not affect the LC/MS profiles of the heparinase II digest of SST0001. However, heparinase I generates the particular tetrasulfated disaccharide I_{2S}-A_{NS3S6S} (not formed by heparinase II treatment) in the starting heparin, recently found in porcine and bovine heparins (Naggi et al., 2016). This fragment is absent in SST0001 (Figs. 4 and S3), most likely because *N*-sulfation is required for the cleavage of this specific sequence by heparinase I.

Chromatographic profiles and corresponding LC/MS data obtained for the heparin and SST0001 samples digested with the heparinase mixture are shown in Fig. 4 and Table 3. An abbreviation system, including in a systematic manner the number of monosaccharide residues, sulfates, acetyl groups and gs-residues when present, was used for each structure identified by LC/MS. The symbol "ΔU" was used to indicate the presence of 4,5-unsaturated uronic acid at the non-reducing end. Symbols "R" and "ol" were used to indicate the presence of a remnant of the hydrolyzed gs-residues and reduced monosaccharide (alditol) at the RE.

The LC/MS profile of the starting heparin digest is mainly composed of disaccharides (most of which were confirmed by injecting standard disaccharides, Fig. 4a) and tetrasaccharides with different sulfation degrees (ΔU4,4,1, ΔU4,5,0, ΔU4,6,0, Fig. 4a), generated from the ATBR-sequences resistant to cleavage (Naggi et al., 2016; Shriver et al., 2000; Yu et al., 2000). As a result of the heparinase specificity, almost all the oligosaccharides detected in the SST0001 digest were even-numbered sequences starting with ΔU_{2S} (4,5-unsaturated 2-O-sulfated uronic acids) at the NRE. The SST0001 profile included some dimers generated from the I_{2S}-sequences as well as tetra-, hexa- and octasaccharides with ΔU_{2S} at the NRE and internal gs-residues (Fig. 4b). Among the disaccharides, the prevalent one was ΔU_{2S}-A_{NAc6S} (ΔU2,2,1). This compound is also present in the heparin digest but in significantly lower amount, as it occurs only rarely within heparin sequences. Disaccharide ΔU2,1,1 was assigned to ΔU_{2S}-A_{NAc} (and not to ΔU-A_{NAc6S}) isomer because non-sulfated uronic acids are incorporated in longer oligosaccharides as gs-residues, for example ΔU4,2,2,1gs (ΔU_{2S}-$A_{NAc(6S)}$-gsU-$A_{NAc(6S)}$). This disaccharide ΔU2,1,1 is the N-acetylated analog of ΔU_{2S}-A_{NS}, present in heparin digests (Wang et al., 2012) and is preserved in N-sulfated gs-heparins (Alekseeva et al., 2013).

As expected, the main tetrasaccharide in SST0001 digest is ΔU4,3,2,1gs (ΔU_{2S}-$A_{\underline{NAc6S}}$-gsU-$A_{\underline{NAc6S}}$) corresponding to ΔU4,5,0,1gs (ΔU_{2S}-$A_{\underline{NS6S}}$-gsG-$A_{\underline{NS6S}}$), prevalent gs-tetrasaccharide found in N-sulfated gs-heparins (Alekseeva et al., 2013). The internal gsU residue was shown to be a gsG (A.A, unpublished work), where ΔU4,5,0,1gs was isolated from the digested gs-porcine mucosal heparin and characterized by LC/MS and NMR (Fig. S4). It is worth noting that ΔU_{2S}-$A_{\underline{NS6S}}$-G-$A_{\underline{NS6S}}$, was also previously found in a heparin digest (Xiao et al., 2011).

Hexasaccharide ΔU6,4,3,2gs (ΔU_{2S}-$A_{\underline{NAc6S}}$-gsU-$A_{\underline{NAc6S}}$-gsU-$A_{\underline{NAc6S}}$) with two subsequent –gsU-$A_{\underline{NAc6S}}$- fragments is more intense in the LC/MS chromatogram than ΔU6,3,3,2gs suggesting that adjacent gsU-residues are present mainly within 6-O-sulfated sequences.

Traces of ΔU2,3,0 (ΔU_{2S}-$A_{\underline{NS6S}}$) and ΔU4,4,1,1gs (ΔU_{2S}-$A_{\underline{(NS)6S}}$-gsU-$A_{\underline{(NAc)6S}}$) (Fig. 4b) indicate that sequences with the residual N-sulfated glucosamines are partially adjacent to gsU within SST0001 chains. The observed data are in agreement with the NMR showing the presence of residual N-sulfated glucosamine A_{NS} (~1.6%, Table 2) as well as conductimetric titration indicating almost complete N-desulfation.

Tetrasaccharide ΔU4,5,2 may correspond to ΔU_{2S}-$A_{\underline{NAc6S}}$-I_{2S}-$A_{\underline{NAc3S6S}}$, where the linkage between A_{NAc6S} and I_{2S} followed by

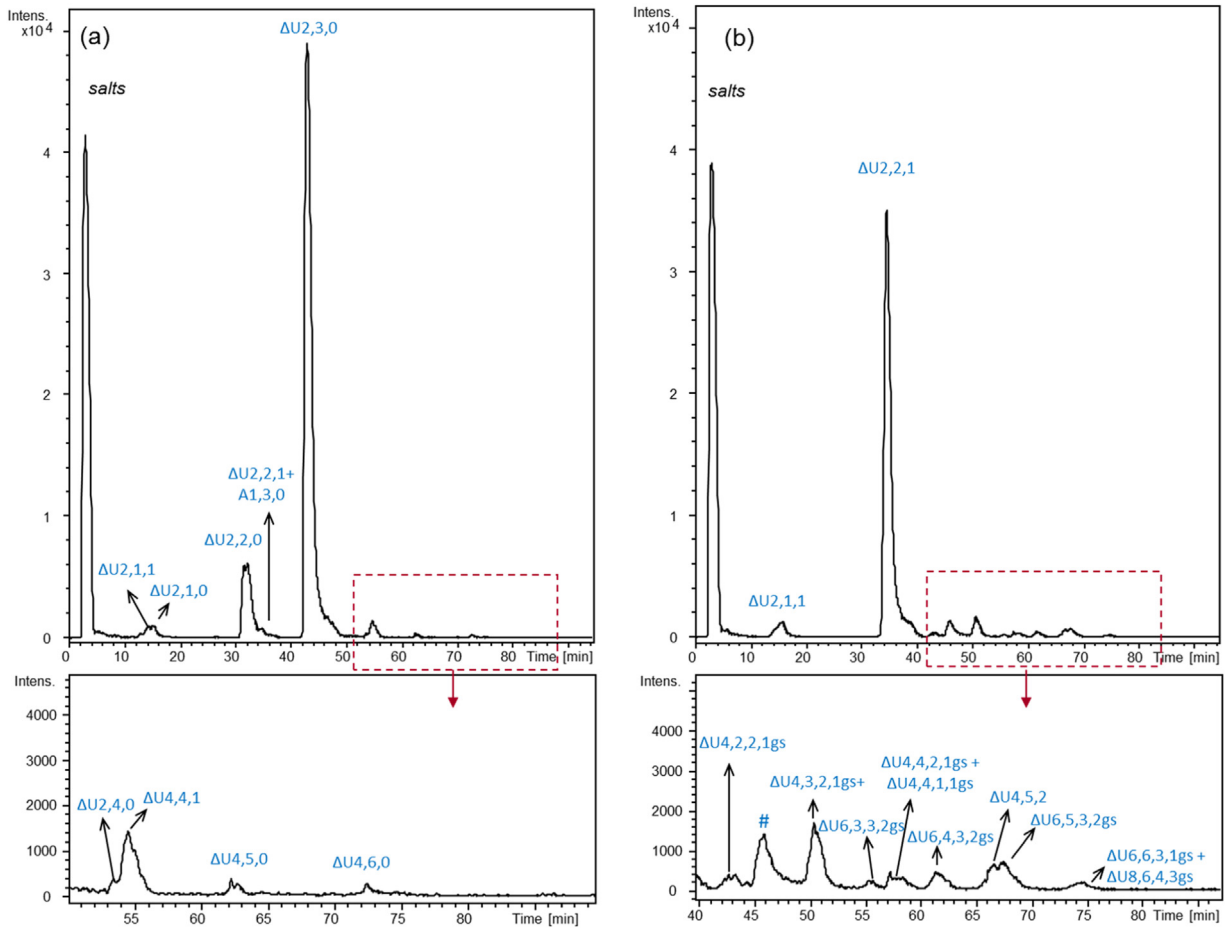

Fig. 4. LC/MS chromatograms of heparin (a) and SST0001 (b) after exhaustive enzymatic digestion with heparinases.
Structures confirmed using disaccharide standards: ΔU2,1,0 (1) = ΔU-A_{NS}, ΔU2,2,0 (1) = ΔU-A_{NS6S}, ΔU2,2,0 (2) = ΔU_{2S}-A_{NS}, ΔU2,2,1 = ΔU_{2S}-A_{NAc6S}, ΔU2,3,0 = ΔU_{2S}-A_{NS6S}
Structures identified based on the LC–MS data and enzyme specificity as well as data published by Naggi et al. (2016): A1,3,0 = A_{NS3S6S}, ΔU2,4,0 = ΔU_{2S}-A_{NS3S6S}, ΔU4,4,1 = ΔU-A_{NAc6S}-G-A_{NS3S6S}, ΔU4,5,0 = $\Delta U_{(2S)}$-$A_{NS(6S)}$-G-$A_{NS3S(6S)}$, ΔU4,6,0 = ΔU_{2S}-A_{NS6S}-G-A_{NS3S6S}.
Peak # does not correspond to an oligosaccharide.
Trace compounds included in Table 3 are not reported in the figure.

a 3-O-sulfated glucosamine is resistant to the heparinases. 3-O-sulfation was deduced to be present at the terminal glucosamine, because the linkage $A_{NAc3S6S}$-I_{2S} is susceptible to heparinase cleavage (NRE-monosaccharide $A_{NAc3S6S}$ was observed in the SST0001 digest). The corresponding N-sulfated tetramer ΔU4,7,0 (ΔU_{2S}-A_{NS6S}-I_{2S}-A_{NS3S6S}) was not found in the heparin digest (Fig. 4a), probably because this N-sulfated sequence is susceptible to enzymatic hydrolysis. In fact, disaccharides ΔU2,3,0 (ΔU_{2S}-A_{NS6S}) and ΔU2,4,0 (ΔU_{2S}-A_{NS3S6S}) are present in the heparin digest (Figs 4a and S3). The resistance of the sequence A_{NAc6S}-I_{2S}-$A_{NAc3S6S}$ (the same as in ΔU4,5,2) to the heparinases could give rise to the mono-gs-hexasaccharide ΔU6,6,3,1gs, which was tentatively assigned to ΔU_{2S}-A_{NAc6S}-gsU-A_{NAc6S}-I_{2S}-$A_{NAc3S6S}$.

As for previously studied gs-heparins (Alekseeva et al., 2013), several ATBR-related gs-oligosaccharides were observed in the SST0001 digest. Hexaccharide ΔU6,5,3,2gs was assigned to ΔU_{2S}-A_{NAc6S}-gsI-A_{NAc6S}-gsG-$A_{NAc3S6S}$ ($[M-2H+2DBA]^{2-}$ m/z 898.72, RT 67.3 min, Table 3) corresponding to the N-sulfated hexamer ΔU_{2S}-A_{NS6S}-gsI-A_{NS6S}-gsG-A_{NS3S6S} found in gs-heparin digests. Tetrasaccharide ΔU4,4,2,1 ΔU_{2S}-A_{NAc6S}-gsG-$A_{NAc3S6S}$ ($[M-2H]^{2-}$ m/z 539.03, RT 57.1 min, Table 3) was likely generated from the N-acetylated highly sulfated variant of ATBR (Loganathan et al., 1990; Naggi et al., 2016).

Several minor components, markers of side reaction, such as hydrolysis, O-acetylation, alditol formation at the RE, were also detected in the SST0001 digest (Fig. 4b). The monoacetylated disulfated disaccharide bearing remnant of gs-uronic acid ΔU2,2,1-R (m/z 656.04, RT 44.3 min, Table 3) indicates that minor hydrolytic side reactions occurred during the SST0001 preparation. Diacetylated and disulfated disaccharide ΔU2,2,2 (m/z 580.028, RT 37.8 min, Table 3), present in trace amounts, suggests that 3-O-acetylation may also occur during the N-acetylation reaction and requires accurate monitoring. The sequence ΔU_{2S}-A_{NAc6S}-gsU-A_{NAc6S}-ol was assigned to the trace tetrasaccharide ΔU4,3,2,1gs-ol (m/z 500.05, RT 50.2 min, Table 3) generated by borohydride reduction or terminal glucosamines of the starting heparin. The presence of alditol fragments at the RE of SST0001 chains was confirmed by exhaustive reduction of SST0001 followed by the enzymatic digestion (data not shown). The appearance of new signals with an additional mass increase of 2 Da would indicate that the unmodified (hemiacetal forms) were present at the RE of the SST0001 chains. However, no difference was found comparing SST0001 and reduced SST0001 digests. This result is in agreement with NMR, showing the absence of the RE amino sugars in the HSQC NMR spectrum of SST0001 (Fig. 3).

LR, a particular RE sequence, present in several heparin chains, can also be susceptible to oxidation, reduction and partial hydrolysis (Alekseeva et al., 2014a). Glucuronic acid (G_{LR}) and xylose (Xyl) within LR, containing vicinal hydroxyl groups, as well as serine were expected to be oxidized by periodate. In fact, NMR spec-

Table 3
LC/MS data for oligosaccharides generated by SST0001 exhaustive digestion with heparinases.

Compound	Prevalent ion form	Calculated monoisotopic *m/z* value	Experimental monoisotopic *m/z* value	Retention time, min
ΔU2,1,1	$[M-H]^-$	458.0610	458.0607	14.5
A1,1,1	$[M-H]^-$	300.0395	300.0390	17.3
Trace				
U2,2,1	$[M-H]^-$	556.0284	556.0305	32.2
Trace				
ΔU2,2,1	$[M-H]^-$	538.0178	538.0183	34.3
A1,2,1	$[M-H]^-$	379.9963	379.9946	34.6
Trace				
ΔU2,2,2	$[M-H]^-$	580.0284	580.0296	37.8
Trace				
ΔU4,2,2,1gs	$[M-2H]^{2-}$	459.0688	459.0701	42.6
ΔU2,3,0	$[M-H]^-$	575.9641	575.9659	43.0
Trace				
ΔU2,2,1-R	$[M-H]^-$	656.0444	656.0446	44.3
Trace				
ΔU4,1,2,1gs-gsLR1	$[M-2H]^{2-}$	766.1988	766.1823	45.9
Trace				
ΔU4,2,2,1gs-gsLR2	$[M-2H]^{2-}$	747.1639	747.1494	46.3
Trace				
ΔU4,3,2,1gs	$[M-2H]^{2-}$	499.0472	499.0500	50.2
ΔU4,3,2,1gs-ol	$[M-2H]^{2-}$	500.0551	500.0460	50.2
Trace				
ΔU4,3,2,1gs-gsLR2	$[M-2H]^{2-}$	787.1423	747.1340	53.9
Trace				
ΔU6,3,3,2gs	$[M-2H]^{2-}$	689.6108	689.6127	55.1
ΔU4,4,2,1gs	$[M-2H]^{2-}$	539.0256	539.0280	57.1
ΔU4,4,1,1gs	$[M-2H]^{2-}$	518.0204	518.0234	58.3
ΔU6,4,3,2gs	$[M-2H]^{2-}$	729.5892	729.5916	61.2
ΔU4,3,2,1gs-gsLR1	$[M-2H]^{2-}$	846.1556	846.1386	61.5
Trace				
ΔU4,5,2	$[M-2H+1DBA]^{2-}$	642.5721	642.5742	66.4
ΔU6,5,3,2gs	$[M-2H+2DBA]^{2-}$	898.7194	898.7236	67.3
ΔU8,5,4,3gs	$[M-2H+3DBA]^{2-}$	1153.8588	1153.8572	69.7
Trace				
ΔU6,6,3,1gs	$[M-2H+3DBA]^{2-}$	1002.2658	1002.2683	74.6
ΔU8,6,4,3gs	$[M-2H+4DBA]^{2-}$	1258.4131	1258.4276	74.3

Trace: intensity lower than 3 * noise.
LR1 = gsG-Gal-Gal-gsXyl-CH_2COOH.
LR2 = gsG-Gal-Gal-$CH(CH_2OH)_2$.

tra show the disappearance of serine residues and chemical shift of G_{LR} and Xyl residues caused by their splitting (Fig. 3). LC/MS results, showing the presence of both gsLR sequences (gsG-Gal-Gal-gsXyl-CH_2COOH and gsG-Gal-Gal-$CH(CH_2OH)_2$, Table 3), support the NMR data about partial hydrolysis of gsXyl.

4. Discussion

4.1. Major and minor structural features of Roneparstat

The results of the present study show that major modifications introduced at each step of SST0001 preparation can be monitored using conductimetric titration, SEC-TDA and monodimensional NMR. Conductimetry and SEC-TDA permits to monitor the completeness of N-desulfation and side reactions. Periodate/borohydride treatment was expected to be one of the most sensitive to various factors, such as pH, temperature, reaction time. However, it was shown that the applied conditions of glycol-splitting provide complete glycol-splitting without significant molecular weight decrease and, consequently, chain hydrolysis.

SEC-TDA can provide evidence for conformational changes occurring during glycol-splitting of heparin. The data reported in Table 1 clearly show that N-acetylated gs-heparin (SST0001) possesses more flexible random coil conformation (lower values of Mark-Houwink parameters *a* and *logK* as well as hydrodynamic radius R_h) than the starting porcine mucosal heparin, due to a lower sulfation degree and the presence of flexible gs-residue joints along SST0001 chains (*see Section* 3.2). Such chain flexibility can facilitate interactions with the heparin/HS binding sites of proteins (Casu & Naggi, 2003), including the recently reported interactions of SST0001 with both heparin binding domains of heparanase (Pala et al., 2016; *see Discussion in Section* 4.2).

In addition to SEC-TDA and conductimetry, NMR represents another important method for SST0001 characterization and Roneparstat preparation monitoring. The parallel application of these methods permitted complementary structural information about major modifications that occur at each step of SST0001 preparation (N-desulfation, N-acetylation, glycol-splitting, hydrolytic side reactions) to be obtained. NMR, in contrast with the other two methods, provides more detailed and accurate data about both major residues and some minor modifications. The monodimensional ^{13}C NMR gives rise characteristic spectra that reflect the major chemical modifications (N-desulfation, N-acetylation, glycol-splitting). Along with better characterization of the analyzed samples at the qualitative level and monitoring cross-peaks markers of each performed chemical reaction, the 2D NMR enabled quantitative analysis (Table 2) as previously developed for heparins (Guerrini et al., 2005). As described in detail in Results, NMR provided quantitative data about the residual N-sulfation of SST0001 as well as free amine groups that may be present in the case of incomplete N-acetylation. Some side reactions, such as hydrolysis of glycosidic bonds and gs-residues, can be also detected by monitoring RE signals and those related to the remnant of uronic acids. 2D NMR provides information concerning monosaccharide composition, including sulfation/acetylation degree and the ratio of I/G and gsI/gsG in heparin and SST0001, respectively, that may be

Table 4
Major and minor structures found within internal sequences and end groups of SST0001 chains.

Sequences within SST0001chains		Corresponding heparinase-generated oligosaccharide
Internal sequences		
I_{2S} regions	**-(I_{2S}-$A_{NAc(6S)}$)$_n$-** R = SO_3^- (prevalently) or H	ΔU2,2,1
gsG/gsI regions	- I_{2S}-A_{NAc6S}-**(gsU-A_{NAc6S})$_n$**-I_{2S} - n = 1 (prevalently) or 2	ΔU4,3,2,1gs ΔU6,4,3,2gs
gsG-$A_{NAc3S6S}$ (gs-ATBR) sequences	-I_{2S}-A_{NAc6S}-gsI-**A_{NAc6S}-gsG-$A_{NAc3S6S}$**-I_{2S} - –I_{2S}-**A_{NAc6S}-gsG-$A_{NAc3S6S}$**-I_{2S} –	ΔU6,5,2,2gs ΔU4,4,2,1gs
I_{2S}-$A_{NAc3S6S}$ containing sequences	–I_{2S}-A_{NAc6S}-**I_{2S}-$A_{NAc3S6S}$**-I_{2S} - –I_{2S}-A_{NAc6S}-gsU-A_{NAc6S}-**I_{2S}-$A_{NAc3S6S}$**-I_{2S} -	ΔU4,5,2 ΔU6,6,3,1gs
Non-reducing end **residues**		
Chains starting with glucosamine	**$A_{NAc3S6S}$**-I_{2S} -	A1,2,1
Chains starting with iduronic acid	**I_{2S}-A_{NAc6S}**-I_{2S} -	U2,2,1
Reducing end **residues**		
Chains with gs-uronic acid followed by a glucosamine in alditol form	-I_{2S}-A_{NAc6S}-**gsU-A_{NAc6S}-ol**	ΔU4,3,2,1gs-ol
Chains with remnant of gs-uronic acid followed by a glucosamine in alditol form	**-I_{2S}-A_{NAc6S}-R**	ΔU2,2,1-R
Chains containing gs linkage region sequences	–I_{2S}-$A_{NAc(6S)}$-gsU-A_{NAc}-**gsG-Gal-Gal-gsXyl-CH_2COOH (gsLR1)** –I_{2S}-$A_{NAc(6S)}$-gsU-A_{NAc}-**gsG-Gal-Gal-CH(CH_2OH)$_2$ (gsLR2)**	ΔU4,1,2,1gs-gsLR1 ΔU4,2,2,1gs-gsLR2 ΔU4,3,2,1gs-gsLR1 ΔU4,3,2,1gs-gsLR2

useful for further structure-activity relationship studies. It is worth noting that the oxidation kinetics of I and G can differ (Alekseeva, Elli, Cosentino, Torri, & Naggi, 2014), so that their quantification is important for controlling periodate oxidation reaction. Control of the completeness of G oxidation is crucial for the Roneparstat activity because the presence of unmodified G may make SST0001 chains maintain affinity for heparanase and be degraded by this enzyme.

Minor modifications and side-reaction markers can be revealed by LC/MS analysis of heparinase digested SST0001, making this approach a necessary step for identification of minor fragments originally present in heparin (e.g., 3-O-sulfated glucosamines, LR sequence, residual N-sulfated glucosamines) or chemically introduced (e.g., N-desulfated and N-acetylated glucosamines, gs-uronic acids, oxidized LR sequence and 3-O-acetylated residues) during Roneparstat preparation. It is worth noting that the applied ion-pair chromatographic separation mode, compatible with ESI–MS, also allows the separation of isomers, providing informative LC/MS profiles of the heparin/SST0001 digests.

The combination of the heparinase specificity with LC/MS analysis of the digestion products allowed to identify major internal and terminal residues present along SST0001 chains. Their internal sequences mainly contain regions without incorporated gs-uronic acids, giving rise to the disaccharides ΔU2,2,1 (Fig. 4) and ΔU2,1,1. The prevalent gs-containing tetrasaccharide ΔU4,3,2,1gs indicates that gs-residues are distributed along the SST0001 chains and interspersed by regular disaccharide blocks, susceptible to heparinase cleavage. Interestingly, residual N-sulfated glucosamines, found by the LC/MS analysis of the SST0001 digest, also appeared adjacent to gs-residues. The few hexa- and octasaccharides, containing two and three subsequent gs-uronic acids, were also found within 6-O-sulfated sequences.

Almost no significant differences were observed between the digestions performed by adding heparinase mixture (heparinases I, II and III) and by using only heparinase II. The only sequence that was not cleaved by this latter was A_{NS6S}-I_{2S}-A_{NS3S6S}. In the case of acetylated SST0001 chains, such a sequence was not cleaved even by the heparinase mixture. The presence of ΔU4,5,2 also indicates that the fragment I_{2S}-A_{NS3S6S} within original heparin chains is followed by sulfated uronic acid (otherwise, it would be present within a gs-oligomer) and mainly preceded by trisulfated disaccharide unit I_{2S}-A_{NS6S}, confirming that this particular sequence is present with highly sulfated regions (Table 4). As for this tetrasaccharide and based on the enzyme specificity, hexasaccharide ΔU6,6,3,1gs was assigned to ΔU$_{2S}$-A_{NAc6S}-gsU-A_{NAc6S}-I_{2S}-$A_{NAc3S6S}$ showing that this peculiar sequence can also be preceded by gs-uronic acid (non-sulfated uronic acid in original heparin) in minor sequences (Table 4).

These results show that the combination of glycol-splitting and specific enzymatic treatment can provide relevant structural information not only about minor particularities in building blocks but also about the structural environment of these particular sequences. The observed highly sulfated environment, along with the other SST0001 properties discussed in 4.2, may play an important role in interaction of gs-chains with various proteins.

The variety of terminal residues of chains present in SST0001 was identified. The traces of A1,2,1 and saturated disaccharide U2,2,1 in the SST0001 digest suggest that SST0001 chains bear both saturated glucosamine and 2-O-sulfated uronic acid at the NRE. The presence of these minor components indicates that the 3,4-vicinal hydroxyl groups at the NRE residues were not affected by glycol-splitting. In contrast, the RE sequences were more susceptible to various steps of the Roneparstat preparation. Borohydride reaction led to the generation of alditol forms at the RE of SST0001 chains (e.g. ΔU4,3,2,1gs-ol in Fig. 4), as result of reduction of hemiacetal residues. These sequences are mainly 6-O-sulfated and a gs-uronic acid precedes terminal glucosamine A-ol. Additionally, several SST0001 chains contain remnants of the gs-uronic acids at the RE, represented by ΔU2,2,1-R in the LC/MS chromatogram (Fig. 4). Several linkage region-containing oligomers were also detected in the SST0001 digest. Table 3 reports both gsLR1 (gsG-Gal-Gal-gsXyl-CH_2COOH, Fig. 1c) and gsLR2 (gsG-Gal-Gal-CH(CH_2OH)$_2$) containing species, indicating susceptibility of this particular RE sequence to hydrolysis. These terminal structures can be used as markers for controlling process of SST0001 preparation.

Altogether, the data obtained provide structural information concerning internal sequences present within SST0001 chains that can be useful for the future investigations of structure – activity

relationship, as well as terminal residues, which can used for monitoring the reproducibility of Roneparstat preparation (Table 4).

4.2. Roneparstat structural features affecting its biological activity

Roneparstat is currently in clinical trials for treatment of advanced multiple sarcoma, however, structure-activity correlations were not studied due to the absence of detailed structural data concerning this drug. The structural features of Roneparstat reported in the present study can indicate the most important directions for future investigations.

The higher conformational flexibility induced in Roneparstat chains by lower sulfation degree (30% lower than for heparin) and gs-residues (from one to three subsequent residues) facilitates interactions with heparin/HS binding proteins. Comparing Roneparstat to the gs-LMWHs under development (Zhou et al., 2011), its high size chains (Mw 16.6 kDa), comparable with unfractionated heparins, may facilitate binding with proteins. This feature could be responsible for the interaction of Roneparstat with heparanase occurring with both of its binding sites or with two heparanase molecules simultaneously (Pala et al., 2016).

One of the key advantages of Roneparstat and other gs-drugs resides in the modification of glucuronic acid that makes these products poor substrates for heparanase and prevents them from degradation and from losing their inhibitory activity. Additionally, the splitting of two uronic acids within the N-acetylated ATBR sequence of some SST0001 chains causes a drop in anticoagulant activity of Roneparstat and, consequently, the absence of side effects associated with these heparin properties.

As mentioned above (Section 4.1), gs-residues are located mainly within 6-O-sulfated sequences, so that electrostatic interactions should play an important role in the interaction of gs-sequences with proteins. However, lower sulfation degree with respect to N-sulfated gs-heparins decreases unspecific interactions with the other proteins, making Roneparstat a more selective drug for the inhibition of heparanase and other proteins, e.g. HGF and VEGF (Ritchie et al., 2011). Recently, Roneparstat anti-tumor efficacy in experimental sarcoma models has been explained by the multitarget inhibition of receptor tyrosine kinases involved in malignant sarcoma signaling pathways (Cassinelli et al., 2016). These effects, likely cooperating with heparanase inhibition, contribute to the anti-tumor efficacy of the drug.

5. Conclusions

The development of efficient and complementary analytical techniques has become increasingly important to structurally characterize complex GAG-based biologically active products, to assist in their derivatization under controlled conditions as well as to help study their interaction with proteins and other biomacromolecules, for the purpose of rationalizing the search of new potential drugs.

In the present study the structural features of the biologically active Roneparstat, being currently studied in clinical trials as non-anticoagulant heparanase-inhibitor, have been studied for the first time.A combination of conductimetric titration, SEC-TDA, NMR and LC–MS analysis of the enzymatically digested samples, provides complementary structural information concerning major and minor internal sequences as well as terminal residues of SST0001 chains.

The internal sequences are represented by a large variety of structures that may play an important role in interactions with proteins. The SST0001 internal domains comprise mainly repeating I_{2S}-A_{NAc6S} disaccharide building blocks interspersed by gs-uronic acids, predominantly one or two subsequent gs-residues. Sequences with three gs-residues were also found but in significantly lower proportion. The observed gs-sequences are expected to provide higher chain flexibility, facilitating interactions with heparanase, growth factors and other proteins involved in tumor development. Notably, gs-sequences are located mainly within 6-O-sulfated sequences that could play an important role in electrostatic interactions and facilitate binding with proteins.

In the present study the variety of the NRE and RE sequences was also determined, e.g. 3-O-acetylated fragments, N-sulfated residual glucosamines, alditol at the reducing end, oxidized linkage region, remnant of the gs-residues. These features represent markers useful for monitoring the reproducibility of Roneparstat preparations, along with sulfation degree and molecular weight.

It is worth noting that parallel analysis of starting heparin helps monitoring structural particularities originally present in heparins and chemical modifications introduced at each step in the preparation of SST0001. The results obtained by combinations of different analytical techniques provide for the first time criteria for structural characterization of Roneparstat. This offers an analytical tool for evaluation of the batch-to-batch reproducibility, necessary for confirming consistency of the clinical trial data where different batches are being tested. Obviously, successful application of the developed analytical methods will require validation studies.

Conflict of interest

There is no potential conflict of interest.

Acknowledgements

The authors gratefully acknowledge financial support from Sigma-tau Research Switzerland S.A (Mendrisio, Switzerland), and thank them for providing Roneparstat drug. The authors also thank Dr. Cesare Cosentino (Ronzoni Institute, Italy) for acquiring NMR spectra and Dr. Giuseppe Cassinelli for the discussion of the results.

Appendix A. Supplementary data

Supplementary data associated with this article can be found, in the online version, at http://dx.doi.org/10.1016/j.carbpol.2016.09.032.

References

Achour, O., Poupard, N., Bridiau, N., Juchereau, S. B., Sannier, F., Piot, J.-M., et al. (2016). Anti-heparanase activity of ultra-low-molecular-weight heparin produced by physicochemical depolymerization. *Carbohydrate Polymers*, *135*, 316–323.

Alekseeva, A., Casu, B., Torri, G., Pierro, S., & Naggi, A. (2013). Profiling glycol-split heparins by high-performance liquid chromatography/mass spectrometry analysis of their heparinase-generated oligosaccharides. *Analytical Biochemistry*, *434*, 112–122.

Alekseeva, A., Casu, B., Cassinelli, G., Guerrini, M., Torri, G., & Naggi, A. (2014). Structural features of glycol-split low-molecular-weight heparins and their heparin lyase generated fragments. *Analytical and Bioanalytical Chemistry*, *406*, 249–265.

Alekseeva, A., Elli, S., Cosentino, C., Torri, G., & Naggi, A. (2014). Susceptibility of enoxaparin reducing end amino sugars to periodate oxidation. *Carbohydrate Research*, *400*, 33–43.

Bertini, S., Bisio, A., Torri, G., Bensi, D., & Terbojevich, M. (2005). Molecular weight determination of heparin and dermatan sulphate by size exclusion chromatography with a triple detector array. *Biomacromolecules*, *6*, 168–173.

Cassinelli, G., Favini, E., Dal Bo, L., Tortoreto, M., De Maglie, M., Dagrada, G., et al. (2016). Anti-tumor efficacy of the heparan sulfate mimic roneparstat (SST0001) against sarcoma models involves multi-target inhibition of receptor tyrosine kinases. *Oncotarget, Advanced Publications*, 1–16.

Casu, B., & Gennaro, U. A. (1975). Conductimetric method for the determination of sulfate and carboxyl groups in heparin and other mucopolysaccharides. *Carbohydrate Research*, *39*, 168–176.

Casu, B., & Lindahl, U. (2001). Structure and biological interactions of heparin and heparan sulfate. *Advances in Carbohydrate Chemistry and Biochemistry*, *57*, 159–206.

Casu, B., & Naggi, A. (2003). Antiangiogenic heparin-derived heparan sulfate mimics. *Pure and Applied Chemistry*, *75*, 157–166.
Casu, B., Vlodavsky, I., & Sanderson, R. D. (2007). Non-anticoagulant heparins and inhibition of cancer. *Pathophysiology of Haemostasis and Thrombosis*, *36*, 195–203.
Casu, B. (2005). Structure and active domains of heparin. In H. G. Garg, R. J. Linhardt, & C. A. Hales (Eds.), *Chemistry and biology of heparin and heparan sulfate* (pp. 1–28). Amsterdam: Elsevier.
Conrad, H. E., & Guo, Y. (1992). Structural analysis of periodate-oxidized heparin. *Advances in Experimental Medicine and Biology*, *313*, 31–36.
Desai, U. R., & Linhardt, R. J. (1995). Molecular weight of heparin using 13C nuclear magnetic resonance spectroscopy. *Journal of Pharmaceutical Sciences*, *84*, 212–215.
Ferro, V., Dredge, K., Liu, L., Hammond, E., Bytheway, I., Li, C., et al. (2007). PI-88 and novel heparan sulphate mimetics inhibit angiogenesis. *Seminars in Thrombosis and Hemostasis*, *33*, 557–568.
Ferro, V., Liu, L., Johnstone, K. D., Wimmer, N., Karoli, T., Handley, P., et al. (2012). Discovery of PG545: A highly potent and simultaneous inhibitor of angiogenesis, tumor growth, and metastasis. *Journal of Medicinal Chemistry*, *55*, 3804–3813.
Fu, L., Li, G., Yang, B., Onishi, A., Li, L., Sun, P., et al. (2013). Structural characterization of pharmaceutical heparins prepared from different animal tissues. *Journal of Pharmaceutical Sciences*, *102*, 1447–1457.
Guerrini, M., Bisio, A., & Torri, G. (2001). Combined quantitative (1)H and (13)C nuclear magnetic resonance spectroscopy for characterization of heparin preparations. *Seminars in Thrombosis and Hemostasis*, *5*, 473–482.
Guerrini, M., Naggi, A., Guglieri, S., Santarsiero, R., & Torri, G. (2005). Complex glycosaminoglycans: Profiling substitution patterns by two-dimensional nuclear magnetic resonance spectroscopy. *Analytical Biochemistry*, *337*, 35–47.
Guerrini, M., Guglieri, S., Naggi, A., Sasisekharan, R., & Torri, G. (2007). Low molecular weight heparins: Structural differentiation by bidimentional nuclear magnetic resonance spectroscopy. *Seminars in Thrombosis and Hemostasis*, *33*, 478–487.
Höök, M., Björk, I., Hopwood, J., & Lindahl, U. (1976). Anticoagulant activity of heparin: Separation of high-activity and low-activity heparin species by affinity chromatography on immobilized antithrombin. *FEBS Letters*, *66*, 90–93.
Iacomini, M., Casu, B., Guerrini, M., Naggi, A., Pirola, A., & Torri, G. (1999). Linkage region sequence of heparin and heparan sulfate: Detection and quantification by Nuclear Magnetic Resonance spectroscopy. *Analytical Biochemistry*, *274*, 50–58.
Langeslay, D. J., Urso, E., Gardini, C., Naggi, A., Torri, G., & Larive, C. K. (2013). Reversed-phase ion-pair ultra-high-performance-liquid chromatography-mass spectrometry for fingerprinting low-molecular-weight heparins. *Journal of Chromatography A*, *1292*, 201–210.
Lever, R., & Page, C. P. (2002). Novel drug development opportunities for heparin. *Nature Reviews Drug Discovery*, *1*, 140–148.
Loganathan, D., Wang, H. M., Mallis, L. M., & Linhardt, R. J. (1990). Structural variation in the antithrombin III binding site region and its occurrence in heparin from different sources. *Biochemistry*, *29*, 4362–4368.
Mousa, S. A., & Petersen, L. J. (2009). Anti-cancer properties of low-molecular-weight heparin: Preclinical evidence. *Thrombosis and Haemostasis*, *102*, 258–267.
Mousa, S. A., Linhardt, R., Francis, J. L., & Amirkhosravi, A. (2006). Anti-metastatic effect of a non-anticoagulant low-molecular-weight heparin versus the standard low-molecular-weight heparin enoxaparin. *Thrombosis and Haemostasis*, *96*, 816–821.
Naggi, A., Casu, B., Perez, M., Torri, G., Cassinelli, G., Penco, S., et al. (2005). Modulation of the heparanase-inhibiting activity of heparin through selective desulfation, graded N-acetylation, and glycol-splitting. *Journal of Biological Chemistry*, *280*, 12103–12113.
Naggi, A., Gardini, C., Pedrinola, G., Mauri, L., Urso, E., Alekseeva, A., et al. (2016). Structural peculiarity and antithrombin binding region profile of mucosal bovine and porcine heparins. *Journal of Pharmaceutical and Biomedical Analysis*, *118*, 52–63.
Naimy, H., Leumarie, N., Bowman, M. J., Costello, C. E., & Zaia, J. (2008). Characterization of heparin oligosaccharides binding specifically to antithrombin III using mass spectrometry. *Biochemistry*, *47*, 3155–3161.
Pala, D., Rivara, S., Mor, M., Milazzo, F. M., Roscilli, G., Pavoni, E., et al. (2016). Kinetic analysis and molecular modelling of the inhibition mechanism of roneparstat (SST0001) on human heparanase. *Glycobiology*, *pii*(cww003)
Pisano, C., Vlodavsky, I., Ilan, N., & Zunino, F. (2014). The potential of heparanase as a therapeutic target in cancer. *Biochemical Pharmacology*, *89*, 12–19.
Ritchie, J. P., Ramani, V. C., Ren, Y., Naggi, A., Torri, G., Casu, B., et al. (2011). SST0001, a chemically modified heparin: Inhibits myeloma growth and angiogenesis via disruption of the heparanase/syndecan-1 axis. *Clinical Cancer Research*, *17*, 1382–1393.
Shriver, Z., Sundaram, M., Venkataraman, G., Fareed, J., Linhardt, R., Biemann, K., et al. (2000). Cleavage of the antithrombin III binding site in heparin by heparinases and its implication in the generation of low molecular weight heparin. *Proceedings of National Academy of Sciences of the United States of America*, *97*, 10365–10370.
Shriver, Z., Capila, I., Venkataraman, G., & Sasisekharan, R. (2012). Heparin and heparan sulfate: Analyzing structure and microheterogeneity. In R. Lever, B. Mulloy, & C. P. Page (Eds.), *Heparin: A century of progress* (pp. 159–176). New York: Springer.
Thanawiroon, C., Rice, K. G., Toida, T., & Linhardt, R. (2004). Liquid chromatography/mass spectrometry sequencing approach for highly sulfated heparin-derived oligosaccharides. *Journal of Biological Chemistry*, *279*, 2608–2615.
Vlodavsky, I., & Friedman, Y. (2001). Molecular properties and involvement of heparanase in cancer metastasis and angiogenesis. *Journal of Clinical Investigation*, *108*, 341–347.
Wagner, H. L. (1985). The Mark-Houwink-Sakurada equation for the viscosity of linear polyethelene. *Journal of Physical and Chemical Reference Data*, *14*, 611–617.
Wang, B., Buhse, L., Al-Hakim, A., Boyne Ii, M. T., & Keire, D. A. (2012). Characterization of currently marketed heparin products: Analysis of heparin digests by RPIP-UHPLC-QTOF-MS. *Journal of Pharmaceutical and Biomedical Analysis*, *67-68*, 42–50.
Wu, L., Viola, C. M., Brzozowski, A. M., & Davies, G. J. (2015). Structural characterization of human heparanase reveals insights into substrate recognition. *Nature Structural and Molecular Biology*, *22*, 1016–1022.
Xiao, Z., Tappen, B. R., Ly, M., Zhao, W., Canova, L. P., Guan, H., et al. (2011). Heparin mapping using heparin lyases and the generation of a novel low molecular weight heparin. *Journal of Medicinal Chemistry*, *54*, 603–610.
Yamada, S., Yamane, Y., Tsuda, H., Yoshida, K., & Sugahara, K. (1998). A major common trisulfated hexasaccharide core sequence: Hexuronic acid (2-sulfate)-glucosamine (N-sulfate)-iduronic acid-N-acetylglucosamine-glucuronic acid-glucosamine (N-sulfate) isolated from the low sulfated irregular region of porcine intestinal heparin. *Journal of Biological Chemistry*, *273*, 1863–1871.
Yates, E. A., Santini, F., Guerrini, M., Naggi, A., Torri, G., & Casu, B. (1996). 1H and 13C NMR spectral assignments of the major sequences of twelve systematically modified heparin derivatives. *Carbohydrate Research*, *294*, 15–27.
Yu, G., LeBrun, L., Gunay, N. S., Hoppensteadt, D., Walenga, J., Fareed, J., et al. (2000). Heparinase I acts on a synthetic heparin pentasaccharide corresponding to the antithrombin III binding site. *Thrombosis Research*, *100*, 549–556.
Zhang, F., Yang, B., Ly, M., Solakyildirim, K., Xiao, Z., Wang, Z., et al. (2011). Structural characterization of heparins from different commercial sources. *Analytical and Bioanalytical Chemistry*, *401*, 2793–2803.
Zhou, H., Roy, S., Cochran, E., Zouaoui, R., Chu, C. L., Duffner, J., et al. (2011). M402, a novel heparan sulfate mimetic, targets multiple pathways in tumor progression and metastasis. *PLos ONE*, *6*, e21106. http://dx.doi.org/10.1371/journal.pone.0021106